nature materials

ARTICLES

PUBLISHED ONLINE: 15 NOVEMBER 2009 | DOI: 10.1038/NMAT2572

Giant Zeeman splitting in nucleation-controlled doped CdSe:Mn^{2+} quantum nanoribbons

Jung Ho Yu[1]*, Xinyu Liu[2]*, Kyoung Eun Kweon[3], Jin Joo[1]†, Jiwon Park[4], Kyung-Tae Ko[5], Dong Won Lee[1], Shaoping Shen[2], Kritsanu Tivakornsasithorn[2], Jae Sung Son[1], Jae-Hoon Park[5], Young-Woon Kim[4], Gyeong S. Hwang[3], Margaret Dobrowolska[2], Jacek K. Furdyna[2]‡ and Taeghwan Hyeon[1]‡

Doping of semiconductor nanocrystals by transition-metal ions has attracted tremendous attention owing to their nanoscale spintronic applications. Such doping is, however, difficult to achieve in low-dimensional strongly quantum confined nanostructures by conventional growth procedures. Here we demonstrate that the incorporation of manganese ions up to 10% into CdSe quantum nanoribbons can be readily achieved by a nucleation-controlled doping process. The cation-exchange reaction of $(CdSe)_{13}$ clusters with Mn^{2+} ions governs the Mn^{2+} incorporation during the nucleation stage. This highly efficient Mn^{2+} doping of the CdSe quantum nanoribbons results in giant exciton Zeeman splitting with an effective *g*-factor of ~600, the largest value seen so far in diluted magnetic semiconductor nanocrystals. Furthermore, the sign of the *s–d* exchange is inverted to negative owing to the exceptionally strong quantum confinement in our nanoribbons. The nucleation-controlled doping strategy demonstrated here thus opens the possibility of doping various strongly quantum confined nanocrystals for diverse applications.

Doping, that is, intentional incorporation of impurities into a material, is the primary means of tuning the electronic, optical and magnetic properties of bulk semiconductors. With the recent emergence of nanoscience and nanotechnology, doping of semiconductor nanocrystals has also attracted a great deal of attention[1–4]. Low-dimensional nanocrystalline materials in the quantum confinement regime (quantum wires or quantum ribbons) are increasingly attracting wide interest owing to their unique properties, arising both from their low dimensionality and their characteristic quantum confinement effects, which hold promise for advanced nanodevice applications[5–7]. The development of new nanoscale doping strategies is naturally critical for the various applications of these low-dimensional quantum structures.

Manganese ion (Mn^{2+})-doped nanocrystals provide excellent model systems for studying the doping process because of their unique magnetic and optical properties, which can be characterized by means of various spectroscopic techniques[1]. Furthermore, from the viewpoint of their applications, doping of non-magnetic semiconductors by transition-metal ions such as Mn^{2+} leads to the formation of diluted magnetic semiconductors (DMSs), which have exotic magnetic and magneto-optical properties, such as the giant Zeeman splitting of electronic states and carrier-induced ferromagnetism, arising from the *sp–d* exchange interaction between the transition-metal ions and the electronic states of the host semiconductor[8–12]. This interaction—and thus also the resulting properties that follow—are expected to increase with quantum confinement[13]. Consequently, the development of the methodology of synthesis of DMS nanostructures in the quantum confinement regime constitutes a giant step towards investigating new spin-based effects, and ultimately for fabricating spintronic devices[14,15].

Bottom-up colloidal chemical approaches for nanocrystal synthesis offer many advantages over top-down physical methods, including the ease of control of the nanostructure sizes and shapes at low temperature, and homogeneous doping without impurity cluster formation[16–18]. Although much progress has been made in the size- and shape-controlling synthesis of semiconductor nanocrystals[19–22], doping semiconductor nanostructures by colloidal chemical routes is still quite challenging[23–30]. For example, the Mn^{2+} ion is very hard to dope into CdSe nanocrystals despite its bulk solubility in the CdSe matrix of nearly 50% (ref. 31). It was reported that nanoscale doping processes are dominated by the surface-adsorption kinetics of impurity ions during the actual growth of the nanostructure, not during its nucleation process[32]. This is because the so-called magic-sized clusters produced at the nucleation stage are too stable to be doped[33]. Furthermore, when the dimensions of the structure are reduced to the strong quantum confinement regime, the impurity ions have an extremely low probability of being adsorbed on the growing nanocrystals, because most of the volume in this limit consists of the magic-sized clusters[12]. Furthermore, the anisotropic crystal morphology of many low-dimensional nanostructured materials makes doping even more difficult[17,32]. Consequently, successful doping of one-dimensional or two-dimensional semiconductor nanocrystals[34,35]—especially in the strong quantum confinement regime—has rarely been reported.

[1]National Creative Research Initiative Center for Oxide Nanocrystalline Materials and School of Chemical and Biological Engineering, Seoul National University, Seoul 151-744, Korea, [2]Department of Physics, University of Notre Dame, Notre Dame, Indiana 46556-5670, USA, [3]Department of Chemical Engineering, University of Texas at Austin, Austin, Texas 78712-0231, USA, [4]Department of Materials Science & Engineering, Seoul National University, Seoul 151-744, Korea, [5]NCRI Center for Cross-coupled Complex Materials Research & Department of Physics, Pohang University of Science and Technology, Pohang 790-784, Korea. *These authors contributed equally to this work. †Permanent Address: Department of Applied Chemistry, Kyungpook National University, Daegu 702-701, Korea. ‡e-mail: furdyna.1@nd.edu; thyeon@snu.ac.kr.

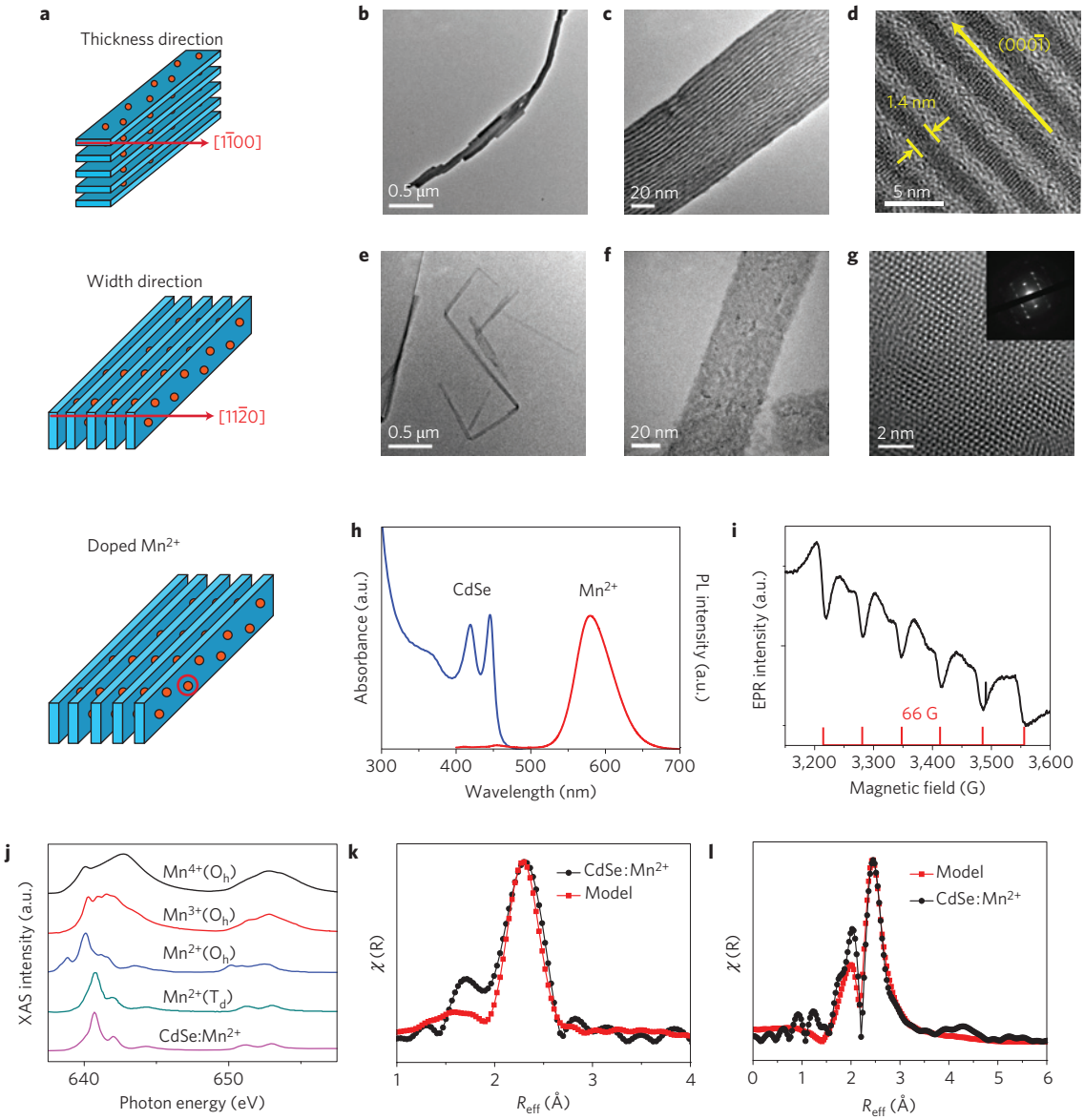

Figure 1 | Synthesis and characterization of CdSe:Mn^{2+} quantum nanoribbons. a, Schematics of CdSe:Mn^{2+} quantum nanoribbon aggregates. **b**–**d**, TEM images of CdSe:Mn^{2+} quantum nanoribbon aggregates, taken along the thickness direction of [1$\bar{1}$00]. The low-magnification (**b**) and the high-magnification (**c**) TEM images taken along the thickness direction, that is, along [1$\bar{1}$00], show that the CdSe:Mn^{2+} quantum nanoribbons are stacked into bundles owing to a strong van der Waals force between successive ribbons. The HRTEM image (**d**) shows that the nanoribbons have a uniform thickness of 1.4 nm, with the growth direction along [000$\bar{1}$] of the wurtzite crystal structure. **e**–**g**, Low-magnification (**e**) and high-magnification (**f**) TEM images and a HRTEM image (**g**) of a single CdSe:Mn^{2+} quantum nanoribbon, taken along the width direction of [11$\bar{2}$0]. The HRTEM image (**g**) and the corresponding selected-area electron diffraction pattern (inset) show that the width direction corresponds to the plane of the wurtzite structure (see Supplementary Fig. S1). **h**–**l**, Characterization of CdSe lattice-incorporated Mn^{2+} ions. The absorption (blue), photoluminescence (red) (**h**), and the EPR spectrum (**i**) show that Mn^{2+} ions are incorporated into the CdSe quantum nanoribbon lattice. The XAS spectrum (**j**) shows that the Mn ions have the oxidation state of (+2) in tetrahedral coordination. Fourier transformed EXAFS, $\chi(R)$, (black circles) at Mn K-edge (**k**) and at Se K-edge (**l**) of CdSe:Mn^{2+} quantum ribbons were fitted with theoretical model calculations (red squares) in the CdSe wurtzite crystal structures.

Here, we demonstrate, however, that when doping can be carried out at the nucleation stage of the nanostructure, this strategy can be very effective for doping even at scales corresponding to strong quantum confinement. Specifically, we show that the cation-exchange reaction of $(CdSe)_{13}$ clusters with Mn^{2+} ions at the nucleation stage, and the subsequent use of those clusters as the building blocks for the desired nanostructure architectures, enable successful doping of Mn^{2+} ions into strongly quantum confining (in our case the 1.4 nm thick) wurtzite-CdSe quantum ribbons, with Mn^{2+} concentrations as high as 10%. This highly efficient Mn^{2+} doping of the CdSe quantum ribbons allowed us to observe a giant Zeeman splitting of excitons (as high as 54.6 meV) and an effective g-factor of ~600, the largest value obtained so far in any DMS nanostructure. Furthermore, owing to the highly uniform thickness (1.4 nm) in the entire CdSe:Mn^{2+} nanoribbon series spanning Mn concentrations varying from 0.7 to 9.4%, we were able to obtain the Zeeman splitting energy as a function of Mn concentration under the same quantum confinement conditions. Our results indicate that the sign of the s–d exchange parameter α in these nanoribbons is inverted to negative owing to the very strong quantum confinement in these II–VI DMS quantum structures. This inversion of the sign of α is consistent

both with recently published experimental results and proposed theoretical models[36–38].

The synthesis of the Mn^{2+}-doped nanoribbons discussed here was carried out by adapting the method for the CdSe nanoribbon synthesis described earlier[39]. The Lewis acid–base reaction of cadmium chloride and manganese(II) chloride with octylammonium selenocarbamate was carried out in octylamine at the low temperature of 70 °C. Transmission electron microscopy (TEM) images show that the synthesized CdSe:Mn^{2+} quantum ribbons have a highly anisotropic morphology with a highly uniform thickness of 1.4 nm, which corresponds to the magic-sized molecular cluster of $(CdSe)_{34}$ (ref. 40), with ribbon widths ranging from 10 to 60 nm, and lengths of a few micrometres (Fig. 1b–g). The high-resolution TEM (HRTEM) image shows that the nanoribbon growth occurred in the [000$\bar{1}$] direction of the wurtzite structure of CdSe (Fig. 1d). Furthermore, the HRTEM images and the corresponding selected-area electron-diffraction images show that the direction normal to the width of the CdSe:Mn^{2+} nanoribbons is the [11$\bar{2}$0] direction of the wurtzite structure (Fig. 1g, Supplementary Fig. S1).

The electronic absorption spectrum of CdSe:Mn^{2+} nanoribbons shows the $1S_h$–$1S_e$ optical transition at 450 nm (2.74 eV), blueshifted by nearly 1 eV from the bulk bandgap of 1.7 eV, that is, showing the effect of strong quantum confinement arising from the extremely small thickness (1.4 nm) of the nanoribbons. Whereas the photoluminescence spectrum of undoped CdSe nanoribbons shows only the blue band-edge emission from the CdSe host[39], the photoluminescence spectrum of the CdSe:Mn^{2+} quantum ribbons shows a suppression of the band-edge emission at 450 nm, and the appearance of a strong emission at 590 nm owing to the pseudo-tetrahedral ($^4T_1$ to $^6A_1$) transition of the Mn^{2+} ions introduced into the CdSe nanoribbons (Fig. 1h). The missing emission from CdSe:Mn^{2+} ribbons might be attributed to the very fast relaxation of the excitons to the Mn excitation in the nanoribbons. The photoluminescence excitation (PLE) spectrum of the 590 nm emission observed in the CdSe:Mn^{2+} quantum ribbons is the same as the optical absorption spectrum, revealing that the energy transfer proceeds from the CdSe quantum ribbon host to the Mn^{2+} ions incorporated in the CdSe lattice (Supplementary Fig. S2). Furthermore, the hyperfine splitting constant obtained from the six-line electron paramagnetic resonance (EPR) spectrum of 1%-doped CdSe:Mn^{2+} quantum nanoribbons is 61.62×10^{-4} cm^{-1}, characteristic of tetrahedrally coordinated Mn^{2+} within the CdSe lattice[32], confirming that Mn^{2+} ions are successfully doped into the 1.4-nm-thick CdSe quantum nanoribbons (Fig. 1i). The X-ray absorption spectrum (XAS) further supports the conclusion that all of the Mn ions are tetrahedrally coordinated with an oxidation sate of (+2), confirming the photoluminescence and EPR data (Fig. 1j). Furthermore, the Mn K-edge and Se K-edge extended X-ray absorption fine structure (EXAFS) spectra show that the effective radii (R_{eff}) of Mn and Se agree well with the theoretically modelled R_{eff} for wurtzite CdSe (Fig. 1k,l), which distinguishes them from the effective radii of Mn and Se in Mn clusters or in α-MnSe clusters (Supplementary Fig. S3), demonstrating that no impurity clusters were formed during the reaction condition. These results are remarkable not only because the Mn^{2+} ions were successfully doped into the ultrathin CdSe quantum nanoribbon host—a notoriously difficult process, as discussed above—but also because shape control of the doped nanocrystals was successfully achieved in the strong quantum-confinement regime by this synthesis process. Furthermore, the elemental analysis based on inductively coupled plasma atomic emission spectroscopy (ICP-AES) reveals that a Mn^{2+} doping concentration as high as 10% was achieved, which corresponds well with the initial $MnCl_2$ concentration under the reaction condition (Table 1, Supplementary Fig. S4).

Table 1 | Comparison of initial molar concentrations of $MnCl_2$ with molar concentrations of Mn^{2+} in the CdSe:Mn^{2+} quantum ribbons, as determined by ICP-AES after washing ten times with pyridine.

$MnCl_2$ initial molar concentration relative to $CdCl_2$ (mol%)	Doped Mn^{2+} concentration confirmed by ICP-AES (mol%)
2.7	2.1 (±0.1)
4	2.5 (±0.4)
5.4	4.1 (±0.5)
6.6	5.8 (±0.5)
8	6.9 (±0.3)
10	8.6 (±0.2)
12	8.8 (±0.3)
14	9.4 (±0.5)
16	9.9 (±0.3)
18	9.9 (±0.4)
20	9.9 (±0.2)

The synthesis was carried out using an intermediate binding amine surfactant[41], which is important for the efficient surface adsorption of the dopant atoms during the growth stage[42]. However, the growth-controlled doping mechanism alone cannot explain the successful very high Mn^{2+} doping of CdSe nanoribbons achieved by the procedure just described, because in previous growth-controlled nanoscale doping methods, less than 10% of the initial precursor concentration has generally been doped into the nanostructures. Furthermore, as the dimensions of the nanocrystals reach the size regime comparable to that of the magic-sized cluster, the impurity atoms are readily expelled rather than being admitted (doped) into the nanocrystals, which is known to result from the characteristic thermodynamic stability of the magic-sized clusters. In the case of CdSe, $(CdSe)_{34}$ clusters are known to be the most abundant and stable nuclei, with a binding energy exceeding 5 eV (ref. 40). One should note here that the thickness of the CdSe:Mn^{2+} quantum ribbons (1.4 nm) is very similar to the size of the magic-sized $(CdSe)_{34}$ clusters.

To understand the formation mechanism of the highly doped CdSe quantum nanoribbons, we measured the optical absorption and photoluminescence of a series of aliquots drawn from the solution during the reaction (Fig. 2). The absorption and photoluminescence spectra taken immediately after the reaction of the metal chlorides with selenocarbamate at ~20 °C correspond to those of the $(CdSe)_{34}$ clusters (Fig. 2a), the main absorption peak at 410 nm corresponding to the $1S_e$–$1S_h$ transition of the $(CdSe)_{34}$ clusters. The photoluminescence spectrum shows a band-edge emission at 450 nm, which is similar to that of the clusters, and a broad emission at around 520 nm, revealing that Mn^{2+} has not been doped into the thermodynamically stable $(CdSe)_{34}$ clusters. As the reaction temperature is raised to ~40 °C, another absorption feature appears at 350 nm, corresponding to $(CdSe)_{13}$ clusters[33,40], and simultaneously the 410 nm peak is seen to decrease (Fig. 2b,c). In the photoluminescence spectrum, the dominant emission appears at 580 nm, which results from the presence of Mn^{2+} ions doped into the CdSe matrix, and the peak at 520 nm is significantly reduced. Moreover, the PLE spectrum of the 580 nm emission reveals that the photoluminescence is associated with the wavelength of 350 nm, and not of 415 nm (Fig. 2d). These absorption, photoluminescence and PLE spectra clearly demonstrate that Mn^{2+} ions are successfully doped into the $(CdSe)_{13}$ clusters, not into the $(CdSe)_{34}$ clusters. When the reaction temperature is further increased to ~60 °C, the absorbance at 410 nm completely disappears, and only the 350 nm absorbance remains (Fig. 2c), whereas only the 580 nm emission remains

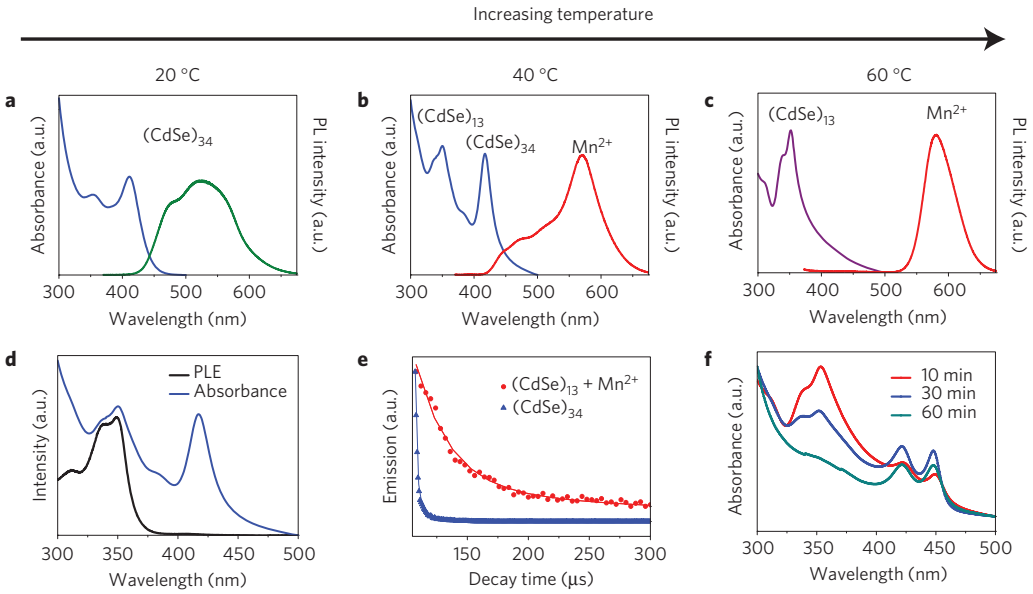

Figure 2 | Spectroscopic investigation of the process of formation and Mn^{2+} doping of CdSe quantum ribbons. a–d, Optical absorption, photoluminescence and PLE spectra of magic-sized clusters formed at the nucleation stage: spectra of $(CdSe)_{34}$ clusters formed at the instant of selenocarbamate injection (**a**); spectra of $(CdSe)_{34}$ and $(CdSe)_{13}$ clusters formed during the heating-up period of the reaction (**b**); spectra of $(CdSe)_{13}$ clusters reacting with Mn^{2+} ions (**c**); absorbance and PLE spectra of 580 nm emission at 40 °C, revealing that $(CdSe)_{13}$ clusters are responsible for the 580 nm emission (**d**). **e**, Time-resolved 580 nm luminescence decays of the reacting mixtures at different stages of reaction. **f**, Absorbance of reacting CdSe:Mn^{2+} mixture during the ageing process at 70 °C.

in the photoluminescence spectrum. Furthermore, time-resolved photoluminescence measurements carried out on this system reveal that the luminescence of $(CdSe)_{34}$ clusters (Fig. 2a) has a lifetime of ~10 μs, whereas the luminescence of $(CdSe)_{13}$ clusters at the wavelength of 580 nm (Fig. 2c) has a much longer lifetime of 274 μs, attributed to the well-known phosphorescence characteristic of the $^4T_1$ to $^6A_1$ transition of Mn^{2+} ions doped inside II–IV semiconductor nanocrystals (Fig. 2e)[43].

In addition, we separately synthesized pure $(CdSe)_{13}$ clusters and $(CdSe)_{34}$ clusters; and we separately reacted a part of these precursor clusters with $MnCl_2$–octylamine complex (see Supplementary Fig. S5). The pure $(CdSe)_{13}$ clusters show a completely different photoluminescence spectrum from the $(CdSe)_{13}$ clusters reacted with $MnCl_2$. Whereas the photoluminescence spectrum of the pure $(CdSe)_{13}$ clusters occurs in the ultraviolet wavelength range with a maximum at 390 nm, the $MnCl_2$-reacted $(CdSe)_{13}$ clusters show a clear pseudo-tetrahedral ($^4T_1$ to $^6A_1$) transition characteristic of Mn^{2+} ions around 580 nm. In stark contrast, there is no significant difference in the photoluminescence spectrum between the pure $(CdSe)_{34}$ clusters and the $MnCl_2$-reacted $(CdSe)_{34}$ clusters. These experimental results further support our view that the Mn^{2+} ions are doped directly into the $(CdSe)_{13}$ clusters, rather than being incorporated by surface adsorption as the nanoribbons are growing.

Thus, the above experimental results suggest that there occurs a cation-exchange reaction of the $(CdSe)_{13}$ clusters with Mn^{2+} ions, whereas this reaction does not occur in the case of the more thermodynamically stable $(CdSe)_{34}$ clusters. As the reaction mixture is further aged at 70 °C, new absorption peaks appear at 420 and 450 nm, which are the characteristic of quantum-well-structured CdSe quantum ribbons, and the 350 nm absorption gradually diminishes and finally disappears (Fig. 2f). These results suggest that the Mn^{2+}-exchanged $(CdSe)_{13}$ clusters act as building blocks in the formation of the 1.4-nm-thick CdSe:Mn^{2+} quantum nanoribbons. Furthermore, we speculate that the extremely high doping concentration of 10% of Mn^{2+} in the 1.4-nm-thick CdSe nanoribbons results from the substitutional replacement of one or two of the Cd^{2+} cations in the $(CdSe)_{13}$ clusters by a Mn^{2+} cation.

To gain a better understanding of the doping of Mn^{2+} ions into the CdSe clusters, first-principle quantum mechanical calculations were carried out (Fig. 3), as follows. For the cation-exchange reaction between Cd^{2+} and Mn^{2+}, we examined three and two distinct sites in the magic-sized clusters $(CdSe)_{13}$ and $(CdSe)_{34}$, respectively; that is, two-fold (indicated as A), three-fold (B) and four-fold (C1 and C2 with slightly different distortions) sites in the former (Fig. 3a), and three-fold (A) and four-fold (B) sites in the latter (Fig. 3b). Taking $MnCl_2$ and $CdCl_2$ as reference species (that is, $(CdSe)_n + MnCl_2 \rightarrow Cd_{n-1}MnSe_n + CdCl_2$), the Cd–Mn exchange tends to be practically thermoneutral ($\Delta H = 0.04$ eV endothermic) at site C1 in $(CdSe)_{13}$. However, the other sites under consideration are predicted to yield sizable endothermicities; that is, 0.27 eV and 0.15 eV at sites A and B in $(CdSe)_{34}$, and 0.17 eV and 0.23 eV at sites A and B in $(CdSe)_{13}$, respectively. Our calculations thus demonstrate the relative ease (from a thermodynamics viewpoint) of Mn incorporation into $(CdSe)_{13}$, as compared with $(CdSe)_{34}$. We also looked at the incorporation of an extra Mn^{2+} into $Cd_{12}MnSe_{13}$ clusters. The second Cd–Mn exchange turns out to be exothermic by 0.08 eV and 0.02 eV when the second Mn^{2+} is placed at sites C2 and A, respectively, with antiferromagnetic coupling to the first Mn^{2+} at site C1, but it becomes noticeably endothermic for ferromagnetic coupling (see Supplementary Fig. S6). The calculation results suggest that more than one Mn^{2+} can be incorporated into the $(CdSe)_{13}$ cluster with preference for antiferromagnetic ordering.

Furthermore, as shown in Fig. 3c, the calculated partial densities of states (PDOS) projected on the 4*p* state of Se atoms and the 5*s* and 4*d* states of Cd atoms in the $(CdSe)_{13}$ cluster show a noticeable shift towards a higher binding energy on Mn incorporation. This suggests that small CdSe clusters can be stabilized by Mn doping. Thus, the computational results are consistent with the experimental observations discussed earlier. This result implies that by controlling the magic-sized cluster synthesis during the nucleation stage, we can control doping at the nucleation stage as well as at the growth stage. The procedure used for the synthesis of CdSe:Mn^{2+} quantum nanoribbons can be readily extended to the

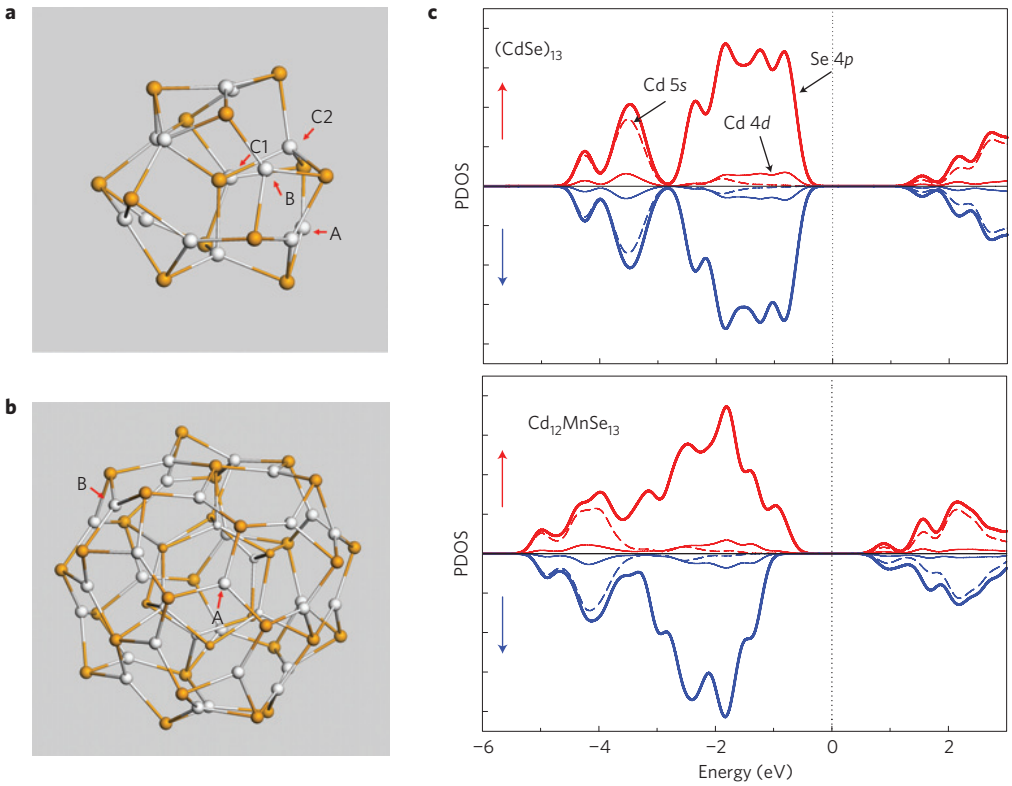

Figure 3 | Theoretical investigation of Mn^{2+} doping of CdSe clusters. a,**b**, Optimized atomic configurations for $(CdSe)_{13}$ (**a**) and $(CdSe)_{34}$ (**b**). The white and yellow spheres represent Cd and Se atoms, respectively. Distinctive Cd sites considered for Cd–Mn exchange are indicated: two-fold (A), three-fold (B) and four-fold (C1 and C2 with slightly different distortions) in $(CdSe)_{13}$, and three-fold (A) and four-fold (B) in $(CdSe)_{34}$. **c**, PDOS for the spin-up (↑) and spin-down (↓) electrons of the Cd and Se atoms. The thick solid lines, thin solid lines and dashed lines represent Se 4*p*, Cd 4*d* and Cd 5*s* states, respectively. The dotted line at $E = 0$ eV indicates the Fermi-level position.

synthesis of other doped II–VI nanoribbons. As an example, we have now also succeeded in synthesizing Mn^{2+}-doped CdS nanoribbons (Supplementary Fig. S7).

Finally, we studied magnetic circular dichroism (MCD) to investigate the *sp–d* exchange interaction of Mn^{2+} ions with electronic states of the host in CdSe:Mn^{2+} nanoribbons in the presence of strong quantum confinement. A strong MCD signal was found at about 2.9 eV (435 nm), which corresponds to the $1S_h$–$1S_e$ interband transition of the optical absorption spectrum. The observation of a large MCD associated with this transition indicates the presence of a giant Zeeman splitting of CdSe excitons owing to the *sp–d* exchange between the band electrons of the CdSe nanoribbon and the incorporated Mn^{2+} ions (Fig. 4a). On the other hand, in this study no MCD was explicitly observed on undoped CdSe nanoribbons in the same magnetic-field regime, even though zero-dimensional CdSe nanocrystals are known to show a small MCD near the exciton transition[44]. The analysis of the MCD data obtained on our Mn-doped CdSe nanoribbons yields a maximum Zeeman splitting of 54.6 meV in the saturation field, and an effective *g*-factor (g_{eff}) of ~600 in the small-field limit (Fig. 4b,d). These values of Zeeman splitting and g_{eff} are the largest seen so far in any DMS nanocrystal system[23,45,46].

The highly uniform size of the nanoribbons with different Mn concentrations in our nanoribbon series allowed us to study the exciton Zeeman splitting as a function of Mn concentration under the same degree of quantum confinement (Supplementary Fig. S8 and Fig. 4c)—a degree of control that is difficult to achieve in DMS quantum wells with ultranarrow thicknesses. From the slope of the Zeeman splitting versus effective Mn concentration (see Supplementary Fig. S9), we obtain the *sp–d* exchange parameter $N_0(\alpha-\beta) = 0.50 \pm 0.10$ eV (Supplementary Fig. S9), yielding the *s–d* exchange constant ($N_0\alpha$) as -0.28 ± 0.10 eV (see Supplementary Information). The calculated value of $N_0\alpha$ is quite surprising, because its sign is opposite to that found in all II–Mn–VI DMSs, where $N_0\alpha$ is positive[8]. Previous reports have shown that the *s–d* exchange interaction in DMS quantum wells is reduced by kinetic exchange between the conduction band electrons and the magnetic ions, leading to the prediction that its sign could be inverted under very strong quantum confinement[47,48]. Recently, it has been reported that g_{eff} could be tunable by the wavefunction engineering of core–shell ZnSe–CdSe nanocrystals, and they suggested that the tunability of the g_{eff} was partly due to the sign inversion of the *s–d* exchange interaction originating from quantum confinement[48]. However, the sign inversion of the *s–d* exchange constant has not been unambiguously confirmed in earlier experiments, most probably because the degree of quantum confinement was insufficient in the DMS-based nanostructures fabricated so far. The dimension of the nanoribbons used in this study allows the electron in the system to experience a very strong confinement (the 1*S* absorption edge blueshifts by nearly 1 eV with respect to bulk CdSe), and at the same time to 'see' a large number of Mn^{2+} ions (which suggests that applying the mean field approximation is probably justified in this case). Under these circumstances, we expect that the model[36], which considers the kinetic exchange between the conduction band electrons and the magnetic ions, can be applied to our nanoribbon system. On the basis of this model, we suggest that the sign reversal of *s–d* exchange arises from the strong quantum confinement. However, even though these conclusions seem convincing to us, several questions definitely need to be addressed. First, the sign inversion of $N_0\alpha$ is predicted on the basis of recent experiments in II–VI DMS quantum wells[36,37,48], as well as by theory[38]. However, the

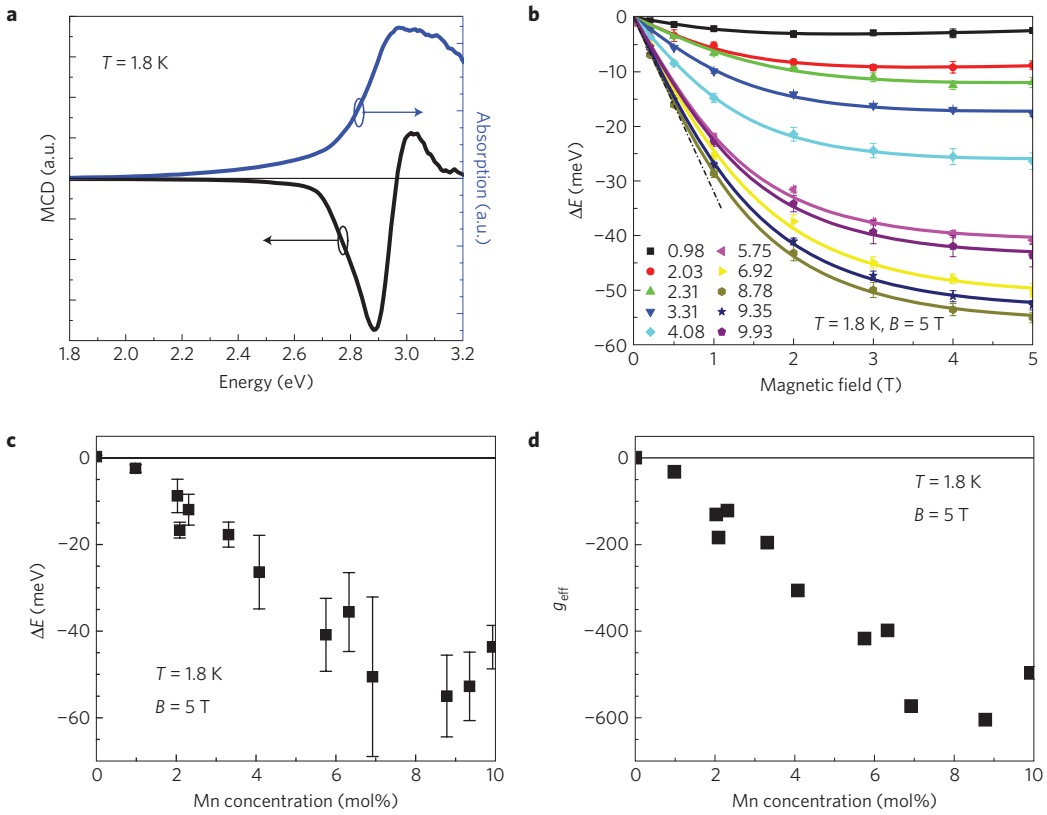

Figure 4 | MCD spectra and corresponding Zeeman splittings of CdSe:Mn^{2+} quantum ribbons. a, The absorption (blue) and MCD spectrum (black) of CdSe:Mn^{2+} quantum ribbons deposited on a sapphire substrate. **b**, Zeeman splitting versus magnetic field for various Mn^{2+} concentrations. **c**, Plot of Zeeman splitting as a function of Mn^{2+} concentration. The error bars represent standard deviations. **d**, Plot of low-field *g*-factor as a function of Mn^{2+} concentration.

applicability of such a prediction in the CdSe:Mn nanoribbon system still needs to be carefully investigated. Second, our results are based on the assumption of an isotropic *g*-factor in the nanoribbon system. However, considering the anisotropic shape of the nanoribbon, we expect that $N_0\alpha$ may experience a much larger change along the strongly quantum confined direction. Third, it has already been reported that for DMS quantum wells one should expect a strong enhancement of magnetic properties in the vicinity of the interface[49]. Consequently, the calculated value of $N_0\alpha$ should strongly depend on the number of Mn clusters on the surface of the nanoribbons. Although the numerical simulation (see Supplementary Information) cannot be expected to rigorously account for the statistics of possible Mn clusters at the surface, the EPR data (Fig. 1i) suggest that the number of Mn clusters on the surface of the nanoribbons seems to be insignificant.

We note parenthetically that the MCD spectra described here were reproducible for several months in a given sample. This attests to the robustness and stability of these nanoribbons, indicating that we can safely ignore the possibility of a self-purification process in this system[50], despite the very narrow thicknesses of the nanoribbons. Thus, because low-dimensional DMS structures can act as spin-transport channels, the controlled assembly of such free-standing robust CdSe:Mn^{2+} quantum ribbons seems to hold promise for new spintronic applications.

Methods

Synthesis of Mn^{2+}-doped CdSe quantum ribbons. The CdSe:Mn^{2+} quantum nanoribbons were synthesized from the reaction of $CdCl_2$ and $MnCl_2$ octylammonium selenocarbamate in octylamine. The octylamine solution of $CdCl_2$ and $MnCl_2$ was prepared by heating 10 ml of octylamine containing 1.5 mmol (0.275 g) of $CdCl_2$ and 0.0075 mmol (0.0094 g) of $MnCl_2$ at 120 °C for 2 h. At this stage, octylamine and $CdCl_2$ reacted to form a mixture of $CdCl_2$(octylamine)$_2$ and $MnCl_2$(octylamine)$_2$ complexes. Octylammonium selenocarbamate was prepared by bubbling CO gas into 5 ml of octylamine containing Se powder (0.355 g, 4.5 mmol), with vigorous stirring for 2 h at room temperature. During this process, the solution colour was gradually changed from black to red brown, finally becoming turbid white. The as-prepared octylammonium selenocarbamate in octylamine was injected into the cadmium–octylamine complex solution at room temperature, instantly generating a transparent light-yellow solution. This solution was slowly heated to 70 °C and kept at this temperature for the desired time. For characterization of the CdSe:Mn^{2+} quantum nanoribbons, aliquots were taken from the reaction mixture during the synthesis of the quantum ribbons. As the quantum nanoribbons were generated, the initially transparent yellow solution changed to turbid yellow. The quantum nanoribbons were then precipitated out by adding excess ethanol containing trioctylphosphine, which was required to remove the un-reacted selenocarbamate.

Magneto-optical spectroscopy. MCD measurements were carried out in a variable-temperature optical cryostat equipped with a 6 T superconducting magnet with magnetic field applied parallel to the direction of light propagation, that is, perpendicular to the surface of the sapphire substrate on which the CdSe:Mn^{2+} nanoribbons are pasted. The MCD measurements were carried out in the transmission mode, using a polarization modulation technique by means of a photoelastic modulator. The transmitted light was detected by a photodiode and lock-in amplifiers.

Received 19 May 2009; accepted 14 October 2009; published online 15 November 2009

References

1. Norris, D. J., Efros, A. L. & Erwin, S. C. Doped nanocrystals. *Science* **319,** 1776–1779 (2008).
2. Talapin, D. V. & Murray, C. B. PbSe nanocrystals solids for n- and p-channel thin film field-effect transistors. *Science* **310,** 86–89 (2005).
3. Shim, M. & Guyot-Sionnest, P. n-type colloidal semiconductor nanocrystals. *Nature* **407,** 981–983 (2000).
4. Yu, D., Wang, C. & Guyot-Sionnest, P. *n*-type conducting CdSe nanocrystal solids. *Science* **300,** 1277–1280 (2003).
5. Xia, Y. *et al.* One-dimensional nanostructures: Synthesis, characterization and applications. *Adv. Mater.* **15,** 353–389 (2003).

6. Yu, H., Li, J., Loomis, R. A., Wang, L.-W. & Buhro, W. E. Two- versus three-dimensional quantum confinement in indium phosphide wires and dots. *Nature Mater.* **2,** 517–520 (2003).
7. Holmes, J. D., Johnston, K. P., Doty, C. & Korgel, B. A. Control of thickness and orientation of solution-grown silicon nanowires. *Science* **287,** 1471–1473 (2000).
8. Furdyna, J. K. & Kossut, J. *Diluted Magnetic Semiconductors; Semiconductors and Semimetals* (Academic, 1988).
9. Awschalom, D. D. & Samarth, N. Spin dynamics and quantum transport in magnetic semiconductor quantum structures. *J. Magn. Magn. Mater.* **200,** 130–147 (1999).
10. Ohno, H. *et al.* Electric-field control of ferromagnetism. *Nature* **408,** 944–946 (2000).
11. Zutic, I., Fabian, J. & Das Sarma, S. Spintronics: Fundamentals and applications. *Rev. Mod. Phys.* **76,** 323–410 (2004).
12. Bryan, J. D. & Gamelin, D. R. Doped semiconductor nanocrystals: Synthesis, characterization, physical properties and applications. *Prog. Inorg. Chem.* **54,** 47–126 (2005).
13. Hoffman, D. M. *et al.* Giant internal magnetic fields in Mn doped nanocrystal quantum dots. *Solid State Commun.* **114,** 547–550 (2000).
14. Yu, D., Wehrenberg, B. L., Yang, I., Kang, W. & Guyot-Sionnest, P. Magnetoresistance of n-type quantum dot solids. *Appl. Phys. Lett.* **88,** 072504–072505 (2006).
15. Liang, W., Yuhas, B. D. & Yang, P. Magnetotransport of Co-doped ZnO nanowires. *Nano Lett.* **9,** 892–896 (2009).
16. Klimov, V. I. *Semiconductor and Metal Nanocrystals* (Dekker, 2004).
17. Yin, Y. & Alivisatos, A. P. Colloidal nanocrystal synthesis and the organic–inorganic interface. *Nature* **437,** 664–670 (2005).
18. Park, J., Joo, J., Kwon, S. G., Jang, Y. & Hyeon, T. Synthesis of monodisperse spherical nanocrystals. *Angew. Chem. Int. Ed.* **46,** 4630–4660 (2007).
19. Murray, C. B., Norris, D. J. & Bawendi, M. G. Synthesis and characterization of nearly monodisperse CdE (E = S, Se, Te) semiconductor nanocrystallites. *J. Am. Chem. Soc.* **115,** 8706–8715 (1993).
20. Peng, X. G. *et al.* Shape control of CdSe nanocrystals. *Nature* **404,** 59–61 (2000).
21. Tang, Z., Zhang, Z., Wang, Y., Glotzer, S. C. & Kotov, N. A. Self-assembly of CdTe nanocrystals into free-floating sheets. *Science* **314,** 274–278 (2006).
22. Robinson, R. D. *et al.* Spontaneous superlattice formation in nanorods through partial cation exchange. *Science* **317,** 355–358 (2007).
23. Norris, D. J., Yao, N., Charnock, F. T. & Kennedy, T. A. High-quality manganese-doped ZnSe nanocrystals. *Nano Lett.* **1,** 3–7 (2001).
24. Hanif, K. M., Meulenberg, R. W. & Strouse, G. F. Magnetic ordering in doped $Cd_{1-x}Co_xSe$ diluted magnetic quantum dots. *J. Am. Chem. Soc.* **124,** 11495–11502 (2002).
25. Stowell, C. A., Wiacek, R. J., Saunders, A. E. & Korgel, B. A. Synthesis and characterization of diluted magnetic semiconductor manganese-doped indium arsenide nanocrystals. *Nano Lett.* **3,** 1441–1447 (2003).
26. Schwartz, D. A., Norberg, N. S., Nguyen, Q. P., Parker, J. M. & Gamelin, D. R. Magnetic quantum dots: Synthesis, spectroscopy, and magnetism of Co^{2+}- and Ni^{2+}-doped ZnO nanocrystals. *J. Am. Chem. Soc.* **125,** 13205–13218 (2003).
27. Zu, L., Norris, D. J., Kennedy, T. A., Erwin, S. C. & Efros, A. L. Impact of ripening on manganese-doped ZnSe nanocrystals. *Nano Lett.* **6,** 334–340 (2006).
28. Magana, D., Petera, S. C., Harter, A. G., Dalal, N. S. & Strouse, G. F. Switching-on superparamagnetism in Mn/CdSe quantum dots. *J. Am. Chem. Soc.* **128,** 2931–2939 (2006).
29. Yang, Y., Chen, O., Angerhofer, A. & Cao, Y. C. On doping CdS/ZnS core/shell nanocrystals with Mn. *J. Am. Chem. Soc.* **130,** 15649–15661 (2008).
30. Pradhan, N., Goorskey, D., Thessing, J. & Peng, X. An alternative of CdSe nanocrystal emitters: Pure and tunable impurity emissions in ZnSe nanocrystals. *J. Am. Chem. Soc.* **127,** 17586–17587 (2005).
31. Mikulec, F. V. *et al.* Organometallic synthesis and spectroscopic characterization of manganese-doped CdSe nanocrystals. *J. Am. Chem. Soc.* **122,** 2532–2540 (2000).
32. Erwin, S. C. *et al.* Doping semiconductor nanocrystals. *Nature* **436,** 91–94 (2005).
33. Soloviev, V. N., Eichhöfer, A., Fenske, D. & Banin, U. Size-dependent optical spectroscopy of a homologous series of CdSe cluster molecules. *J. Am. Chem. Soc.* **123,** 2354–2364 (2001).
34. Yuhas, B. D., Zitoun, D. O., Pauzauskie, P. J., He, R. & Yang, P. Transition-metal doped zinc oxide nanowires. *Angew. Chem. Int. Ed.* **45,** 420–423 (2006).
35. Chin, P. T. K., Stouwdam, J. W. & Janssen, R. A. Highly luminescent ultranarrow Mn doped ZnSe nanowires. *Nano Lett.* **9,** 745–750 (2009).
36. Merkulov, I. A. *et al.* Kinetic exchange between the conduction band electrons and magnetic ions in quantum-confined structures. *Phys. Rev. Lett.* **83,** 1431–1434 (1999).
37. Myers, R. C., Poggio, M., Stern, N. P., Gossard, A. C. & Awschalom, D. D. Antiferromagnetic *s–d* exchange coupling in GaMnAs. *Phys. Rev. Lett.* **95,** 017204 (2005).
38. Bhattacharjee, A. K. Confinement-induced reduction of the effective exchange parameters in semimagnetic semiconductor nanostructures. *Phys. Rev. B* **58,** 15660–15665 (1998).
39. Joo, J., Son, J. S., Kwon, S. G., Yu, J. H. & Hyeon, T. Low-temperature solution-phase synthesis of quantum well structured CdSe nanoribbons. *J. Am. Chem. Soc.* **128,** 5632–5633 (2006).
40. Kasuya, A. *et al.* Ultra-stable nanoparticles of CdSe revealed from mass spectrometry. *Nature Mater.* **3,** 99–102 (2004).
41. Pradhan, N., Reifsnyder, D., Xie, R., Aldana, J. & Peng, X. Surface ligand dynamics in growth of nanocrystals. *J. Am. Chem. Soc.* **129,** 9500–9509 (2007).
42. Du, M.-H., Erwin, S. C. & Efros, A. L. Trapped-dopant model of doping in semiconductor nanocrystals. *Nano Lett.* **8,** 2878–2882 (2008).
43. Suyver, J. F., Wuister, S. F., Kelly, J. J. & Meijerink, A. Luminescence of nanocrystalline ZnSe:Mn^{2+}. *Phys. Chem. Chem. Phys.* **2,** 5445–5448 (2000).
44. Kuno, M., Nirmal, M., Bawendi, M. G., Efros, A. L. & Rosen, M. Magnetic circular dichroism study of CdSe quantum dots. *J. Chem. Phys.* **108,** 4242–4247 (1998).
45. Beaulac, R. *et al.* Spin-polarizable excitonic luminescence in colloidal Mn^{2+}-doped CdSe quantum dots. *Nano Lett.* **8,** 1197–1201 (2008).
46. Hundt, A., Puls, J. & Henneberger, F. Spin properties of self-organized diluted magnetic $Cd_{1-x}Mn_xSe$ quantum dots. *Phys. Rev. B* **69,** 121309 (2004).
47. Kossut, J. Low-dimensional structures of diluted magnetic (semimagnetic) semiconductors-a subjective review. *Acta Phys. Pol. A* **100,** 111–138 (2001).
48. Bussian, D. A. *et al.* Tunable magnetic exchange interactions in manganese-doped inverted core–shell ZnSe–CdSe nanocrystals. *Nature Mater.* **8,** 35–40 (2009).
49. Grieshaber, W. *et al.* Magneto-optic study of the interface in semimagnetic semiconductor heterostructures: Intrinsic effect and interface profile in CdTe–$Cd_{1-x}Mn_xTe$. *Phys. Rev. B* **53,** 4891–4904 (1996).
50. Dalpian, G. M. & Chelikowsky, J. R. Self-purification in semiconductor nanocrystals. *Phys. Rev. Lett.* **96,** 226802 (2006).

Acknowledgements

We would like to thank the National Creative Research Initiative Program (T.H. and J.P.) and the World Class University Program (T.H. and J.P.) of the Korean Ministry of Education, Science and Technology, the US National Science Foundation (J.K.F.) and the Robert A. Welch Foundation (G.S.H.) for financial support. We gratefully acknowledge the Texas Advanced Computing Center for use of their computing resources. We thank M.-S. Won in Korea Basic Science Institute for the EPR characterization. We also thank K. Ando for the preliminary study on MCD. J.H.Y. has benefited from a Seoul Science Fellowship.

Author contributions

J.H.Y., X.L., J.K.F. and T.H. designed and carried out experiments, analysed data and wrote the manuscript. K.E.K. and G.S.H. carried out the quantum mechanical calculations and described the results. J.H.Y., J.J., D.W.L. and J.S.S. carried out the synthesis of the materials. J.P. and Y.-W.K. carried out TEM measurements. K.-T.K. and J.-H.P. conducted XAS and EXAFS. X.L., S.S., K.T., M.D. and J.K.F. carried out magneto-optical experiments and interpreted the data. All authors have reviewed, discussed and approved the results and conclusions of this article.

Additional information

The authors declare no competing financial interests. Supplementary information accompanies this paper on www.nature.com/naturematerials. Reprints and permissions information is available online at http://npg.nature.com/reprintsandpermissions. Correspondence and requests for materials should be addressed to J.K.F. or T.H.